energies

Article

High Refractive Index Diphenyl Sulfide Photopolymers for Solar Cell Antireflection Coatings

Jingran Zhang [1,2], Baozhu Li [3,†], Heran Song [1], Chen Zhao [1,*], Songfeng Liang [1], Zhurong Dong [1,*] and Jie Yu [2]

[1] Research Institute of New Energy Vehicle Technology, Shenzhen Polytechnic, Shenzhen 518055, China; zhangjingran@szpt.edu.cn (J.Z.); songheran@szpt.edu.cn (H.S.); ling@szpt.edu.cn (S.L.)
[2] Key Laboratory of Optoelectronic Chemical Materials and Devices of Ministry of Education, Jianghan University, Wuhan 430056, China; yuhao@szemi.cn
[3] Zhuhai Fudan Innovation Institute, Zhuhai 518057, China; tiger_1984@yeah.net
* Correspondence: zhaochen@szpt.edu.cn or zhaochen913@163.com (C.Z.); arondong@szpt.edu.cn (Z.D.)
† Baozhu Li is the co-first author.

Abstract: The anti-reflection film can effectively reduce the surface reflectivity of solar photovoltaics, increase the transmittance of light, and improve the photoelectric conversion efficiency. The high refractive index coating is an important part of the anti-reflection film. However, the traditional metal oxide coating has poor stability and complicated processes. To address this issue, we prepared two organic high refractive index (HRI) photopolymers by modifying epoxy acrylic acid with 4,4′-thiodibenzenethiol, which can be surface patterned by nanoimprinting to prepare antireflection coatings. As a result, two modified photopolymers with high refractive index (n > 1.63), high optical transmittance (T > 95%), and thermal stability (T_g > 100 °C) are obtained after curing. In particular, the diphenyl sulfide photopolymer modified by ethyl isocyanate acrylate has a refractive index up to 1.667 cured by UV light. Our work confirms that the organic HRI photopolymer can be obtained by introducing high molar refractive index groups, with potential to be applied as a PV cell power conversion efficiency material.

Keywords: refractive index; photopolymer; antireflection coatings; nanoimprinting; solar cells

check for updates

Citation: Zhang, J.; Li, B.; Song, H.; Zhao, C.; Liang, S.; Dong, Z.; Yu, J. High Refractive Index Diphenyl Sulfide Photopolymers for Solar Cell Antireflection Coatings. *Energies* **2022**, *15*, 3972. https://doi.org/10.3390/en15113972

Academic Editors: Yanzhou Qin, Yulin Wang, Xiao Ma and Adalgisa Sinicropi

Received: 12 April 2022
Accepted: 25 May 2022
Published: 27 May 2022

Publisher's Note: MDPI stays neutral with regard to jurisdictional claims in published maps and institutional affiliations.

Copyright: © 2022 by the authors. Licensee MDPI, Basel, Switzerland. This article is an open access article distributed under the terms and conditions of the Creative Commons Attribution (CC BY) license (https://creativecommons.org/licenses/by/4.0/).

1. Introduction

Solar power generation is a sustainable and clean energy source, and an important way to obtain green hydrogen energy [1]. The surface packaging material for transmittance of photovoltaic (PV) cells directly affects the PV light harvesting which converts incoming solar photons to charge carriers [2]. In this way, transferring as much light as possible into the cell can effectively improve the power conversion efficiency (PCE) [3]. Therefore, antireflection coatings (ARCs) are applied on the surface of PV modules to suppress Fresnel surface reflection losses. A single-layer low-refractive-index coating is the simplest anti-reflection coating [4]. Recently, alternating layers of high-low refractive index films [5] have also been reported for anti-reflection coatings, possessing a wider absorption bandwidth and a range of incident angles to improve the short-circuit current of solar cells.

High refractive index photopolymers (HRIPs) are high refractive index polymers (n > 1.5) that can be quickly cured under ultraviolet light (UV) irradiation [6]. This polymer has been widely investigated for potential application in the field of advanced optical device manufacturing, such as lenses [7], optical adhesives [8], holographic lenses [9], intraocular lenses [10], anti-reflective coatings [11], and LED packaging materials [12,13]. The refractive index affects the propagation path of light; the higher the refractive index, the thinner the material can be [14]. Therefore, high refractive index polymers have attracted extensive attention due to the lightweight design requirements of advanced optical devices.

According to the Lorentz-Lorenz equation [15–17], the introduction of substituents with high molar refraction and low molar volume can effectively increase the refractive

index of photopolymer [18]. Benzene ring, sulfur atoms, phosphorus, beryllium, selenium [19,20], and halogen atoms (except fluorine atoms) with higher molar refractivity can increase the refractive index of the polymer. Ueda and colleagues have systemically synthesized and characterized a series of sulfur-containing HRIPs, and found that steric hindrance and molecular packing also affect the refractive index of polymers [21]. In addition, the introduction of nitrogen can increase the hydrogen bond density of the polymer to improve the refractive index [22]. Many groups and atoms such as polysulfide [23], cyclic sulfide [24], biphenyl [25], thianthrene [26], polyimide [27], poly(thiophosphate)s [28], phenyl sulfide [29], carbazole [30,31], pyrimidine [30,31], fluorene [32], sulfone [21] and triazines [33] have been widely studied to improve the refractive index of polymers.

Excessive doping of these functional elements can deepen the color of the polymer, reduce optical transmission, or create problems of insolubility and poor processability.

Nano-composite high refractive index photopolymers are inorganic-organic hybrid materials with high molar refractivity inorganic nanoparticles, such as ZrO_2 [34], ZnS [35], SiO_2 [36,37], and TiO_2 [6,38,39]. Sol-gel is a common surface treatment method reported to improve the compatibility of inorganic-organic composite. The surface of nanoparticles and organics are connected by chemical bonds, the composite HRIPs are transparent, and the refractive index can be increased to 1.8. However, nanoparticles have issues of aggregation, poor processability and low homogeneity [40]. Thus, the composite nanofilms prepared by sol-gel have high roughness and porosity, which limit their application.

Therefore, regardless of organic or inorganic nanomaterials, the application prospect of the final products is still determined by their storage stability, film-forming properties, and optical transmission. Photopolymers are often prepared by using acrylate/methacrylate modified monomers. The photopolymers prepared in this way have outstanding properties such as good compatibility, good film formation, short curing time and high optical clarity [41], and this is a common synthetic route for some advanced optical materials. However, this method will inevitably affect the refractive index of the product. Isocyanate acrylate has isocyanic acid and C=C bond structure, which can replace acrylate to react with functional monomers and introduce C=C bonds that can be light cured. At the same time, the acrylate/methacrylate modified monomers can increase the hydrogen bond density of the light-cured resin and improve its refractive index.

In the present work, the diphenyl sulfide epoxy resins are modified by acrylic acid and isocyanate ethyl acrylate to prepare photopolymers with high refractive index and high optical transmission. We finally succeed in obtaining two liquid diphenyl sulfide photopolymers with a high refractive index ($n > 1.63$). Compared with acrylates, the photopolymer modified with isocyanate acrylate has high optical transmittance, thermal stability, and good film formation. The photopolymer was prepared into antireflection coatings (ARCs) by a facile nanoimprinting technology, which proved its promising application prospects.

2. Materials and Methods

2.1. Materials

Epichlorohydrin (ECH, 99.7%), 4,4′-Thiodibenzenethiol (TDBT, 98%), acrylic acid (AA, 99%, contains 180–200 ppm MEHQ stabilizer), 2-isocyanatoethylacrylate (AOI, 98%), tetrabutylammonium bromide (TABA, 99%), triphenylphosphine (TPP, 99%), ditin butyl dilaurate (DBTDL, 95%), 4-methoxyphenol (MEHQ, 99%) and photoinitiator-1173 (PI-1173, 97%) were purchased from Aladdin Reagent Co., Ltd. (Shanghai, China) without further purification. Low Refractive Index Resin (H819@ QUINSON) and PET film ($n = 1.5$) were purchased from Jincheng Technology Co., Ltd. (Shenzhen, China) and Zhonglian Electronic Material Co., Ltd. (Changshu, China), respectively.

2.2. Synthesis of Thiodibenzenethiol Epoxy Resin

Diglycidyl ether of thiodibenzenethiol epoxy resin (DGETDBT) was synthesized in two steps as shown in Figure 1, and the reaction route was the same as reported work in [26]. The detailed process is shown in Figures 1 and 2.

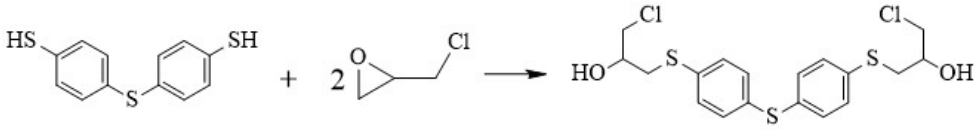


Figure 1. Synthesis of DGETDBT (step 1).

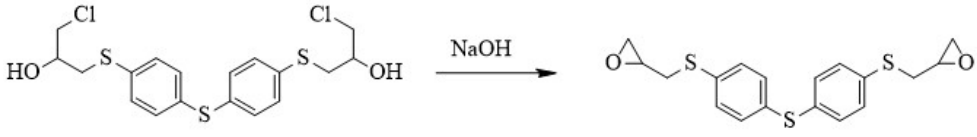


Figure 2. Synthesis of DGETDBT (step 2).

4,4-thiobisbenzenethiol (50 g, 0.2 mol) was stirred to dissolve epichlorohydrin (155 mL, 2 mol) in a 500 mL single-necked round-bottom flask. Then tetra-n-butylammonium bromide (TABA, 0.05 g) was added to the solution. The mixture reacted under a nitrogen atmosphere with continuous stirring at 80 °C for 4 h. At the end of the reaction, the unreacted epichlorohydrin was separated from the product using a rotary evaporator at 60 °C, and a pale-yellow liquid was obtained (step 1).

The pale-yellow liquid was dissolved again by methyl isobutyl ketone (250 mL), then NaOH (8 g, 0.2 mol) was added to the dissolved solution and the mixture reacted for 2 h at 60 °C under a nitrogen atmosphere. After the reaction, NaOH was filtered out using a Brinell funnel (∅ = 150 mm). To separate the methyl isobutyl ketone from the product, the filtrate was vacuum distilled at 60 °C and the product was an orange oil. The oil was washed to neutrality by adding a certain amount of potassium dihydrogen phosphate and deionized water (50 °C), and then the product was separated from the water by extraction with ethyl acetate at 30 °C. The extracted product was evaporated at 60 °C, and 30 g of diphenyl sulfide epoxy resin was obtained (step 2).

To remove impurities from the resin product and further purify the resin, the product DGETDBT of step 2 needs to be purified. First, diphenyl sulfide epoxy resin (30 g) was completely dissolved in 300 mL of anhydrous ethanol at 50 °C, and then the solution was left to recrystallize at −5~0 °C for 6 h. After recrystallization, the crystals were quickly separated by filtration with ethanol in a Buchner funnel at an ambient temperature of 10 °C. Then the product was separated by silica gel column chromatography purification and eluted with dichloromethane/methanol solution. Finally, the solution was spin-dried to obtain 25 g of purified diphenyl sulfide epoxy resin for subsequent reactions.

2.3. Synthesis of EA-UV

The process is shown in Figure 3. Triphenylphosphine (0.01 g, 0.1 wt%) and 4-methoxyphenol (0.01 g, 0.1 wt%) were dissolved in the purified diphenyl sulfide epoxy resin (10 g). The resin mixture was heated in a three-necked flask with constant stirring. When the temperature rose to 75 °C, acrylic acid (5.76 g, 0.08 mol) was added dropwise to the resin within 30 min through a dropping funnel. After the addition of drops, the mixture in the flask was warmed up to 80 °C and the reaction was carried out under light-proof and nitrogen atmosphere conditions for 6 h to obtain ((thiobis(4,1-phenylene)) bis(sulfanediyl)) bis(2-hydroxypropane-3,1-diyl) diacrylate (EA-UV) photopolymer.

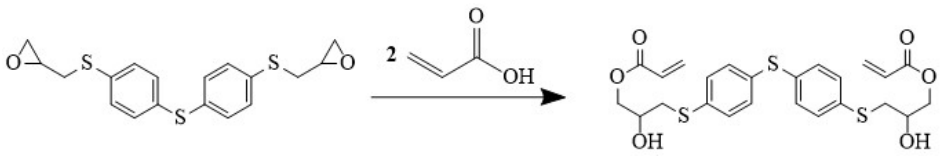


Figure 3. Synthesis of EA-UV photopolymer.

2.4. Synthesis of AOI-UV

The process is shown in Figure 4. Dibutyltin laurate (0.02 g, 0.2 wt%) and 4-methoxyphenol (0.01 g, 0.1 wt%) were dissolved in the purified diphenyl sulfide epoxy resin (10 g). The resin mixture was heated in a three-necked flask with constant stirring. When the temperature rose to 75 °C, ethyl isocyanate acrylate (9.58 g, 0.068 mol) was added dropwise to the resin via a dropping funnel within 30 min. After that, the mixture in the flask was heated to 85 °C and the reaction was carried out under light and nitrogen atmosphere for 6 h to obtain ((((thiobis(4,1-phenylene)) bis(sulfanediyl)) bis(meth-ylene)) bis(2-oxooxazolidine-5,3-diyl)) bis(ethane-2,1-diyl) diacrylate (AOI-UV) photopolymer.

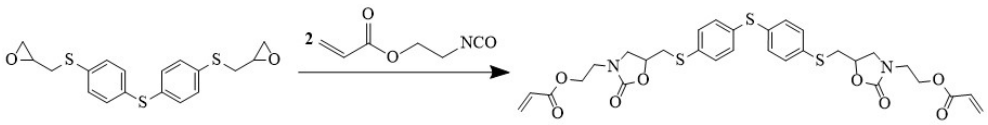


Figure 4. Synthesis of AOI-UV photopolymer.

2.5. Preparation of Film

Photoinitiator-1173 (0.3 wt%) was added into photopolymers (EA-UV/AOI-UV), and then the photocurable resin can be obtained after stirring in the dark at room temperature for 30 min. Photocurable resin was dropped onto a clean glass and scraped into a continuous 25 μm coating with SZQ squeegee. After 1 min of irradiation with 365 nm UV light, the films with thicknesses of 25 μm were successfully prepared and used for better refractive index, transmittance and thermal properties [42].

2.6. Preparation of ARCs Film

Antireflection coatings (ARCs) [43] consists of a specialized optical clear film offering broadband spectral range, reducing the reflection of ambient light on the display interface and improving the light-harvesting in photovoltaic (PV) cells' surface.

The embossing process of the film is shown in Figure 5. The Si mold was placed on the cradle of the nano-imprinter, and 1.5 mL photocurable HRIP was dropped onto the surface of the mold, and then the PET film was covered on the surface of the HRIP to avoid air bubbles. Next, a UV-enabled NIL using a Nanonex NX-B200 was applied, where the pattern duplication occurred when the HRIP was embossed at a certain pressure and then cured using UV light before demolding. After HRIP demolding, low refractive index photopolymer (H819@ Quinson) was dropped onto the pattern surface of the cured HRIP film, and then the PET film was covered on the surface of the photopolymer. Repeat the above embossing procedure to finally obtain high-low refractive index composite ARCs.

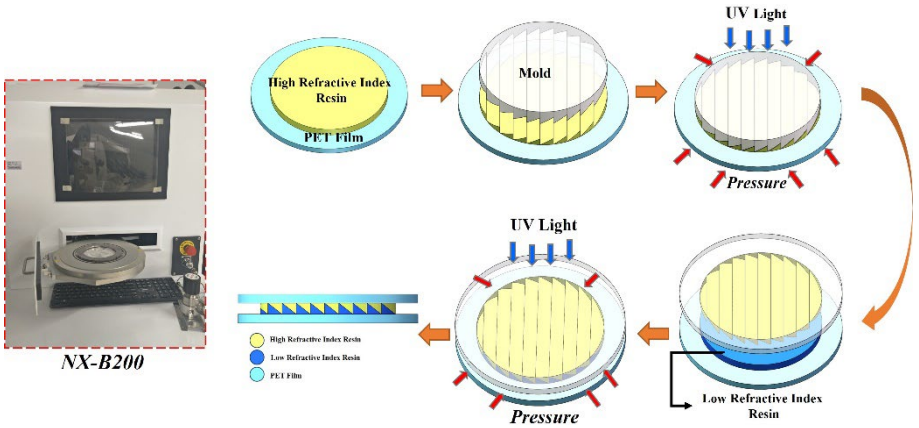


Figure 5. Process diagram of preparing ARCs film using nanoimprinting.

The embossing and molding procedure used is: Step 1, air in the empty bin was extracted by a vacuum pump, then low-pressure nitrogen (100–110 PSI) was filled into it, and the upper and lower covers of the bracket were pushed together (30 s); Step 2, high-pressure nitrogen was filled into the bin, and the pressure was gradually increased to 200 PSI within 1 min; Step 3, high-pressure nitrogen was maintained for 1 min, and the UV resin was completely laminated to the mold to start imprinting; Step 4, 365 nm UV-LED lamp was turned on and light curing was performed for 1 min [44].

2.7. Testing and Characterization

The ^{1}H-NMR spectra of the monomers were recorded on a Bruker Magnet System AV400 MHz spectrometer in $CDCl_3$-d. The sample mass was not less than 8 mg, the sampling time was 2.11 s, and the number of scans was 18 [45].

Fourier transform infrared (FT-IR) spectroscopy (KBr pellets) was recorded on a Bruker TENSOR 27 spectrometer. By comparing the change in the characteristic peak of the product in the range of 4000~500 cm^{-1}, the group change during the reaction can be determined [46].

In order to check the thermal stability of the photopolymer, thermogravimetric analysis was performed on a NETZSCH-TG209F3 TGA thermal analyzer with 5~8 mg film samples heated in flowing nitrogen (flow rate = 40 mL/min) at a heating rate of 10 °C/min from 30 °C to 800 °C [47].

The samples were measured twice on a DSC Q20 TA Instrument at a heating rate of 20 °C/min under a nitrogen atmosphere from 40 °C to 280 °C, with the first heating to eliminate heat history and the second heating to measure T_g [48].

The refractive index of the cured photopolymer film was measured by abbe-3L refractometer (Type WYA-2W from Shanghai Optical Instrument Co., Shanghai, China). The measuring range of the refractometer is n = 1.300~1.700.

Before testing, the refractive index of deionized water was measured to calibrate the refractometer. After calibration, to avoid bubbles between the film and the prism, bromonaphthalene was used as the contact liquid to fully adhere to the prism. The object was measured several times (at least three samples for each object) to calculate the average value [49].

A Shimadzu Spectrophotometer UV-2550 was also used for testing the transmission of the photopolymer film with the thickness of 25 μm, and the measurement range of the wavelength was between 200 nm and 900 nm [50].

Surface SEM images of the samples were obtained by applying a 3 kV voltage. A Hitachi Field Emission Scanning Electron Microscope SU8010 was used to conduct membrane tests and get results. When observing the cross section, the film needed to be brittle fractured by liquid nitrogen [51].

3. Results and Discussion

3.1. Synthesis and Characterization of Photopolymers

As shown in Figure 6a, high refractive index diphenyl sulfide photopolymers were synthesized in two steps. First, epoxy resin was obtained by modifying 4′4-thiobisthiophenol with epichlorohydrin. Then two high refractive index light photopolymers EA-UV and AOI-UV were obtained by modifying the epoxy resin with acrylic acid and isocyanate ethyl acrylate. In the following, the chemical structures of epoxy resin, EA-UV and AOI-UV were confirmed by ^{1}H-NMR spectroscopies [52] and FT-IR spectroscopy. The results of ^{1}H-NMR spectroscopies have been moved to supporting information.

The epoxy resin, EA-UV and AOI-UV photopolymers were tested by FTIR spectroscopy to compare the structural changes before and after the substance reaction.

The FTIR spectra of DGETDBT epoxy resin and its monomer TDBT are shown in Figure 6b. There is an absorption peak at 2600 cm^{-1} in the spectrum line of TDBT for its S-H functional group, whereas the same peak is not found in that of DGETDBT, which suggests that TDBT has been converted completely. The characteristic peaks of the three-member ring ether group at 927 cm^{-1} and the peak representing the stretching vibration of C-O-C at 1267 cm^{-1} of DGETDBT are both sought out in its FTIR spectrum. Further-

more, the characteristic peaks of benzene ring skeleton vibration appear at 1448 cm^{-1} and 3000~3100 cm^{-1}, indicating that diphenyl sulfide has been connected to epichlorohydrin. The appearance of a broad absorption peak at 3474 cm^{-1} and the characteristic peak of water at 1631 cm^{-1} indicate that a small amount of water has been absorbed by DGETDBT, as reported by Anton et al.

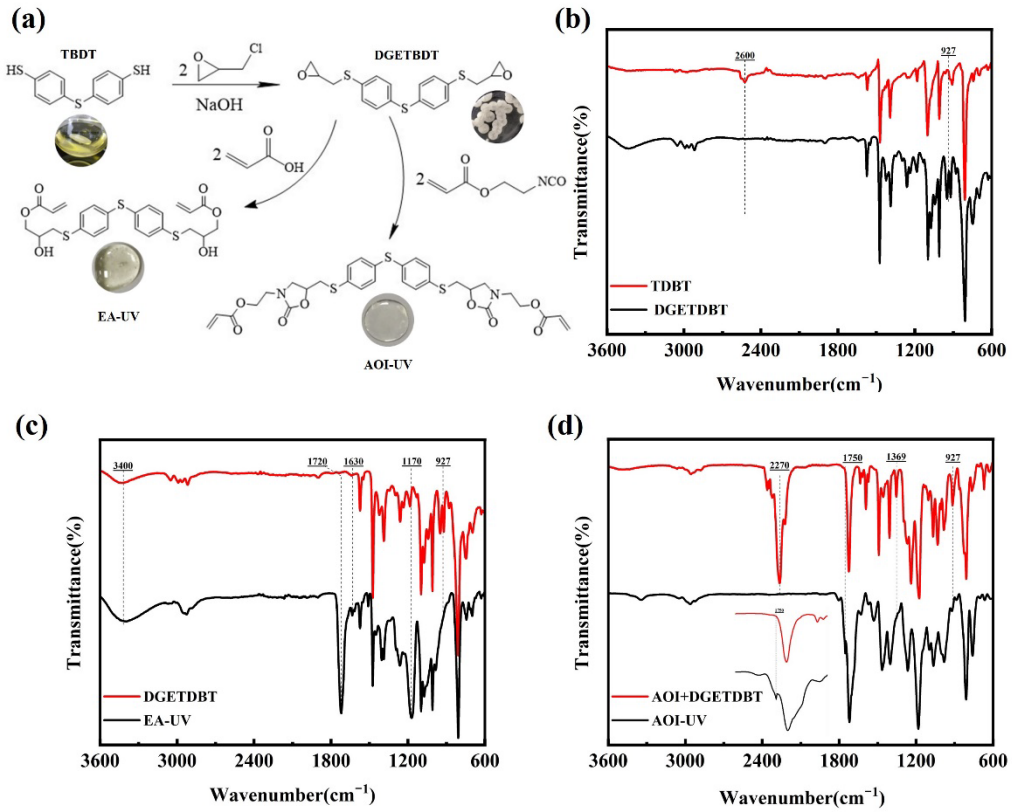


Figure 6. Synthesis and characterization of photopolymers. (**a**) Synthesis of photopolymers. (**b**) FTIR spectra of DGETDBT. (**c**) FTIR spectra of EA-UV. (**d**) FTIR spectra of AOI-UV.

The FTIR spectra of UV-EA photopolymer and its monomer DGETDBT are given in Figure 6c. By comparing the characteristic peaks of the products, it is found that the characteristic peak of DGETDBT epoxy resin at 921 cm^{-1} has disappeared. The product EA-UV shows a characteristic peak of C=O at 1720 cm^{-1} and a peak of C=C at 1630 cm^{-1}. In addition, the area of the carbonyl peak at 3400 cm^{-1} increases, which indicates that acrylic acid has already been esterified with epoxy resin [53].

After DGETDBT was modified by ethyl isocyanate (AOI), the change spectrum of its characteristic peak is shown in Figure 6d. The characteristic peak of the three-member ring ether group disappears at 927 cm^{-1}, but the C=C peak appears at 1630 cm^{-1}. The characteristic peaks of AOI of -N=C=O at 2270 cm^{-1} and -O-C=N- at 1369 cm^{-1} disappear, and the O=C-N< peak representing oxazolidinone appears at 1750 cm^{-1}. This is the same as the results reported in [54], which proves that the epoxy group and the isocyanate group have fully reacted, and a C=C bond-terminated diphenyl sulfide epoxy isocyanate light-curable resin containing an oxazolidinone structure is formed.

3.2. Thermal Properties

Glass transition temperature (T_g) and thermal decomposition temperature (T_d) are important parameters in the design and production of optical devices. According to the experimental method in Section 2.6, two groups of high-refractive photopolymers were tested by DSC and thermogravimetric analysis in the form of 25 μm films.

The DSC test results of the cured films of the two photopolymers are shown in Figure 7. The T_g of the EA-UV photopolymer is 107 °C, and the T_g of the AOI-UV photopolymer is 116 °C. The results indicate that the structure of oxazolidinone has improved the thermal performance of photopolymers.

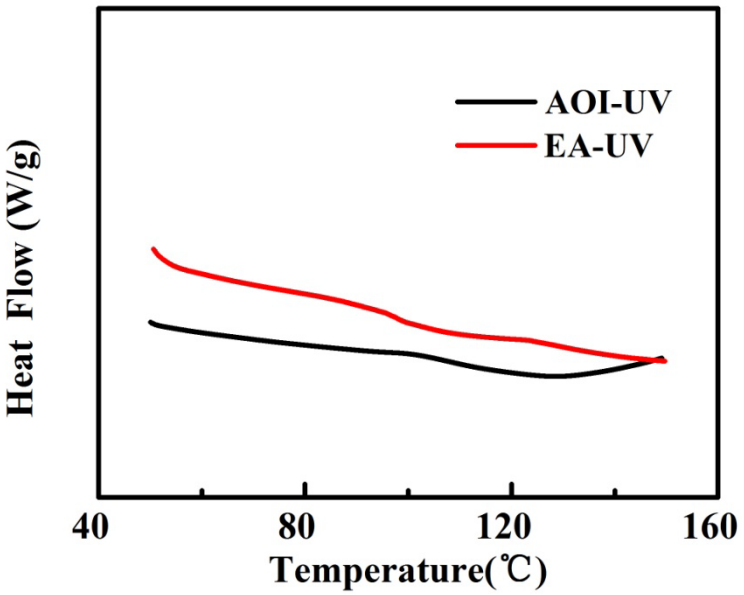


Figure 7. DSC curves of high refractive index UV cured film.

The results of the thermogravimetric analysis are shown in Figure 8 and Table 1. The results show that the EA-UV photopolymer film has two thermal weight loss steps, and part of the prepolymer decomposes at 180 °C to 200 °C. The oxazolidinone structure of the AOI-UV photopolymer film can improve the heat resistance of the polymer [55]. The temperature of 1% thermal weight loss is 209.40 °C, which is 55 °C higher than that of EA-UV resin. However, the main structure of both is diphenyl sulfide, so there is a 10% heat loss around 290~300 °C, and the maximum thermal weight loss rate is between 370 °C and 382 °C.

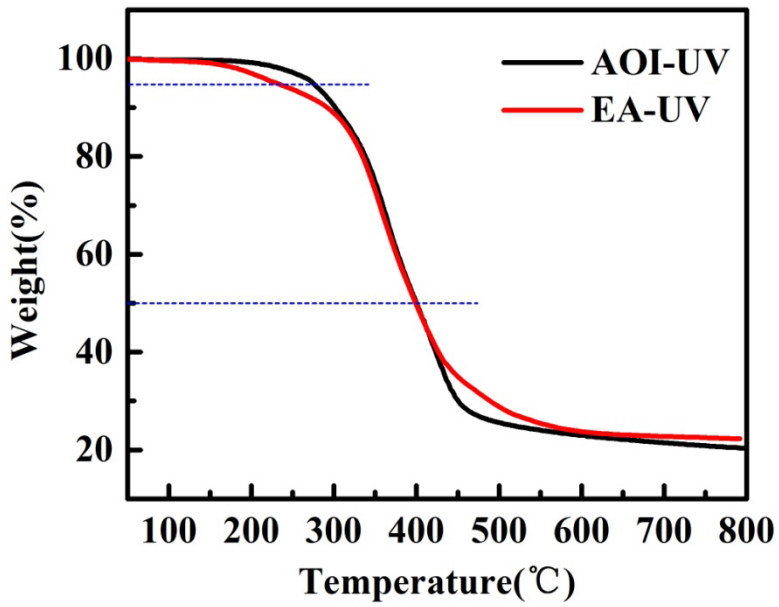


Figure 8. Thermal weight loss curves of high refractive index films.

Table 1. Thermal weight loss test results of two high refractive index UV cured films.

Film	T_1/°C	T_5/°C	T_{10}/°C	T_{50}/°C	D_{TG}/°C	Residue @600 °C
EA-UV	153.60	230.21	291.70	396.39	370.73	20.36%
AOI-UV	209.40	274.42	301.80	400.31	382.38	23.00%

In general, AOI-UV resin contains a five-membered heterocyclic structure of oxazolidinone, so it has a higher crosslink density after curing [56], and its thermal performance is improved compared to EA-UV.

3.3. Optical Properties

The diphenyl sulfide structure with high molar refractive index will make the polymer film show a certain color, which will affect the display effect. Therefore, the optical transparency of the film in the visible region is a key factor in the field of optical applications.

According to the method described in Section 2.7, the optical transmittance and refractive index of the films cured with two high refractive index resins (EA-UV and AOI-UV) were tested using ultraviolet spectrometer and Abbe refractometer, respectively.

The test results are shown in Figure 9 and Table 2. The EA-UV film has a refractive index of 1.633, with UV cut-off wavelength of 328 nm, a transmittance of 95.38% at 450 nm, and the maximum transmittance of 99.83%. The AOI-UV film has a refractive index of 1.667, with UV cut-off wavelength of 318nm, a transmittance of 97.9% at 450 nm and the maximum transmittance of 99.86%.

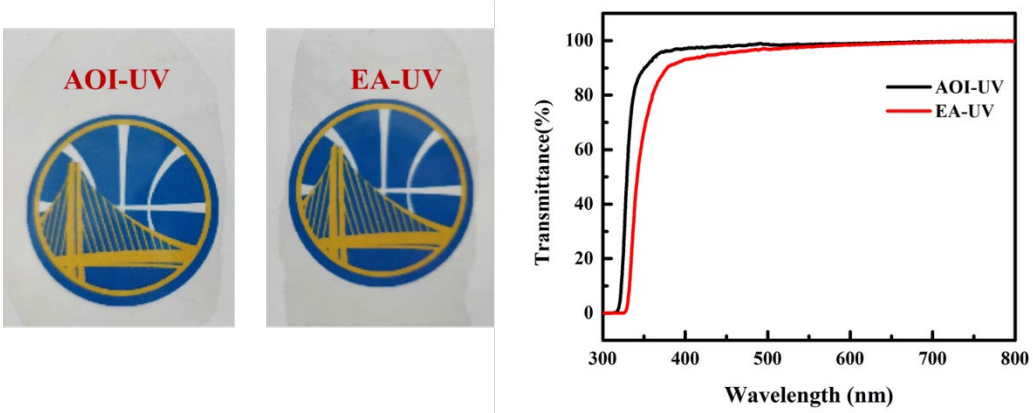


Figure 9. Comparison of optical transmission and photographs of high refractive index cured films.

Table 2. Comparative transmittance and refractive index of UV-curable films.

Film (25 μm)	$\lambda_{cut\text{-}off}$ (nm) [1]	T_{450} (%) [2]	T_{max} (%) [3]	Refractive Index
EA-UV	328	95.38	99.83	1.633
AOI-UV	318	97.9	99.86	1.667

[1] cut-off wavelength in UV_{-vis} transmission spectrum. [2] the transmittance at 450 nm in UV_{-vis} transmission spectrum. [3] the maximum transmittance in UV_{-vis} transmission spectrum.

In particular, the molar refractive index of the AOI-UV is higher than -C-C- because of the large amount of -C-N< bonds contained in the isocyanate modification [57], which also increases the hydrogen bond density of the resin and results in a higher refractive index of AOI-UV relative to EA-UV.

3.4. The Structure of ARCs Films

Antireflection coatings (ARCs), by multiple reflections of light within the yellow absorbing layer (high refractive index), in turn enable the absorption of obliquely incident

ambient light. The display light emitted within the viewing angle range can be transmitted. The basic principle is shown in Figure 10. Controlling the refractive index and structural parameters of each layer can achieve low reflection of oblique incident light [58].

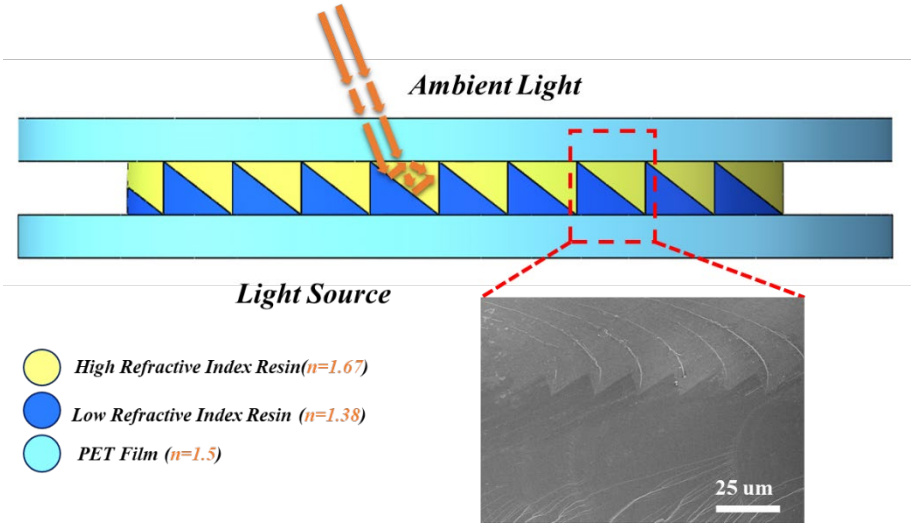


Figure 10. Demonstration of light propagation in ARCs.

First, according to the optical properties of each material, the light transmittance, refractive index, and thermal stability of AOI-UV were better than EA-UV, so AOI-UV was selected as a high refractive index light-curing resin to prepare an ARCs film. Additional PET film and low refractive index resin were selected from mature products in the market, and the final film parameters for each layer are shown in Table 3.

Table 3. Refractive index and structural parameters of each layer of ARCs.

Film	*n*	Transmittance	Critical Angle of Reflection	
PET	1.5	≥93%		
Yellow Layer	1.67	≥97%	69.639°	56.758°
Blue Layer	1.38	≥93%		

With reference to the optical parameters of each layer, the incidence angle of each surface in the case of oblique incidence was calculated, and the size and angle of the microstructure were designed according to the requirement of total reflection [59]. The results show that total reflection on both surfaces can be achieved at $\beta + 25.375^\circ \geq 56.758^\circ$ and $2 \times \beta + 25.375^\circ \geq 69.636^\circ$. In other words, $\beta \geq 31.383^\circ$ can make the light fully reflected in the yellow absorbing layer achieve absorption.

Therefore, ARCs films were prepared using the above angularly designed mold referring to the method described in Section 2.6. The SEM observation was performed on the high refractive film with a single impression and the high-low-refractive film with two impressions. As shown in Figure 11b, the high refractive index resin has a better release, high image integrity and a significant prism angle after resin curing. Figure 11a indicates that the single-layer high refractive resin after nanoimprinting shows the rainbow film phenomenon at different angles. This shows that the prismatic structure and high refractive index of the embossing produce interference with light.

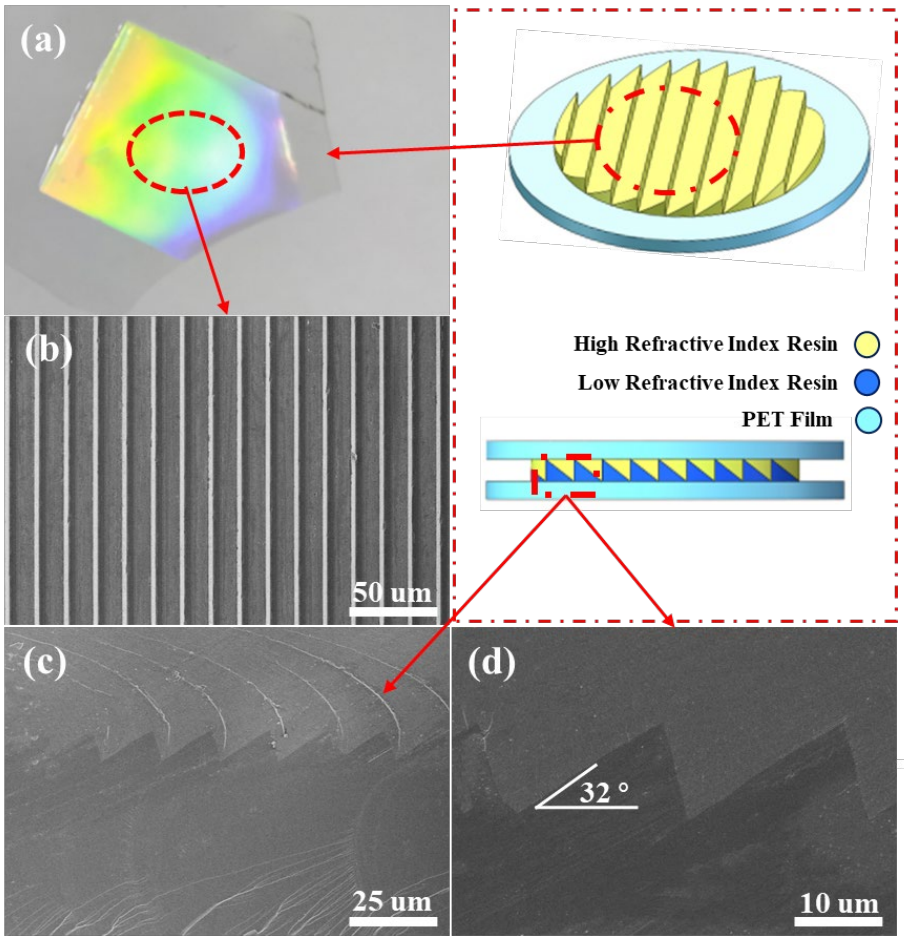


Figure 11. Microstructure and display effect of ARCs. (**a**) Display effect of single-layer high refractive resin after nanoimprinting. (**b**) SEMs of single-layer high refractive resin after nanoimprinting. (**c**,**d**) Microstructure of high-low refractive index composite ARCs films.

High-low refractive index composite ARCs films were obtained by nanoimprinting the low-refractive index resin onto the patterned side of the high-refractive index film. The cross-section of the film was observed using SEM, and the results are shown in Figure 11c,d. The high and low refractive index resins are tightly fit, the overall embossing effect is good, the prism structure is obvious, and the angle is clear and greater than 32°, in accordance with the expected design.

4. Conclusions

In this paper, high refractive index epoxy resins with diphenyl sulfide structure were prepared by the reaction of highly active hydrogen of -SH with epichlorohydrin. Two high refractive index and high optical transmission photopolymers were prepared through the modification of epoxy resins with acrylic acid and isocyanate, and the structure of the both products were verified by FTIR and ^{1}H-NMR.The soft, colorless and transparent films were obtained by curing two photopolymers, which have excellent optical properties in the visible region, especially with optical transmittance over 95% at 450 nm, and the refractive index over 1.63. Besides, both films exhibited good thermal stability with glass transition temperatures above 100 °C and 1% thermal weight loss temperatures above 150 °C.

In particular, the refractive index of AOI-UV films with oxazolidinone structure was up to 1.667, and 1% thermal weight loss temperatures were all above 200 °C. This indicated that the oxazolidinone structure and hydrogen bonding contributed to the improvement of the refractive index and thermal stability of the photopolymer.

Finally, AOI-UV photopolymer with excellent thermal properties, high refractive index and optical transmittance was prepared into well-structured and fully patterned prismatic gratings film using a nano-imprinting technique and antireflection coatings (ARCs) principle. The effect of AOI-UV photopolymer in the molding of micro and nano structures was explored, and the results showed that the photopolymer was well suited as optical film for applications in advanced electronic devices and optical equipment.

Supplementary Materials: The following supporting information can be downloaded at: https://www.mdpi.com/article/10.3390/en15113972/s1, Figure S1: ^{1}H-NMR spectra of DGETDBT; Figure S2: ^{1}H-NMR spectra of EA-UV; Figure S3: ^{1}H-NMR spectra of AOI-UV.

Author Contributions: Conceptualization, J.Y.; Data curation, J.Z., B.L. and S.L.; Investigation, J.Z.; Methodology, C.Z.; Project administration, C.Z.; Software, J.Z.; Supervision, Z.D.; Visualization, J.Z.; Writing—original draft, J.Z.; Writing—review & editing, H.S. All authors have read and agreed to the published version of the manuscript.

Funding: This research received no external funding.

Institutional Review Board Statement: Not applicable.

Informed Consent Statement: Not applicable.

Data Availability Statement: Not applicable.

Acknowledgments: This work was financially supported by the School level scientific research start-up project (6022312004K) and Post-doctoral Later-stage Foundation Project of Shenzhen Polytechnic (6021271009K).

Conflicts of Interest: The authors declare no conflict of interest.

References

1. Da, Y.; Xuan, Y.; Li, Q. From light trapping to solar energy utilization: A novel photovoltaic–thermoelectric hybrid system to fully utilize solar spectrum. *Energy* **2016**, *95*, 200–210. [CrossRef]
2. Gbashi, K.R. Investigation of morphological, optical and structural properties of multi-layer coatings for solar energy. *Appl. Phys. A* **2020**, *126*, 275. [CrossRef]
3. Leem, J.W.; Choi, M.; Yu, J.S. Multifunctional Microstructured Polymer Films for Boosting Solar Power Generation of Silicon-Based Photovoltaic Modules. *ACS Appl. Mater. Interfaces* **2015**, *7*, 2349–2358. [CrossRef] [PubMed]
4. Lin, T.-X.; Chen, K.-J.; Chen, P.-Y.; Jan, J.-S. Broadband Antireflection Coatings Based on Low Surface Energy/Refractive Index Silica/Fluorinated Polymer Nanocomposites. *ACS Appl. Nano Mater.* **2018**, *1*, 741–750. [CrossRef]
5. Hou, G.; García, I.; Rey-Stolle, I. High-low refractive index stacks for broadband antireflection coatings for multijunction solar cells. *Sol. Energy* **2021**, *217*, 29–39. [CrossRef]
6. Hu, X.; Yao, B.; Liu, J.; Liu, J.; Chen, K.; Yan, M.; Wang, L. Preparation and properties of high refractive index UV-cured titanium hybrid optical materials. *Mater. Lett.* **2020**, *265*, 127466. [CrossRef]
7. Zhang, Y.; Wang, Y.; Chen, Y.; Yang, Z.; Chen, M.; Qin, Z. High-refractive index polythiourethane resin based on 2,3-bis((2-mercaptoethyl) thio)-1-propanethiol and 1,3-bis(isocyanantomethyl) cyclohexane using tertiary amine catalyst. *J. Appl. Polym. Sci.* **2020**, *138*, 50278. [CrossRef]
8. Park, C.Y.; Choi, B. Enhanced Light Extraction from Bottom Emission OLEDs by High Refractive Index Nanoparticle Scattering Layer. *Nanomaterials* **2019**, *9*, 1241. [CrossRef]
9. Cody, D.; Gribbin, S.; Mihaylova, E.; Naydenova, I. Low-Toxicity Photopolymer for Reflection Holography. *ACS Appl. Mater. Interfaces* **2016**, *8*, 18481–18487. [CrossRef]
10. Badur, T.; Dams, C.; Hampp, N. High Refractive Index Polymers by Design. *Macromolecules* **2018**, *51*, 4220–4228. [CrossRef]
11. Koshelev, A.; Calafiore, G.; Pina-Hernandez, C.; Allen, F.I.; Dhuey, S.; Sassolini, S.; Wong, E.; Lum, P.; Munechika, K.; Cabrini, S. High refractive index Fresnel lens on a fiber fabricated by nanoimprint lithography for immersion applications. *Opt. Lett.* **2016**, *41*, 3423–3426. [CrossRef]
12. Bari, G.A.R.; Kim, H. High-refractive-index and high-barrier-capable epoxy-phenoxy-based barrier film for organic electronics. *Polym. Adv. Technol.* **2020**, *31*, 1752–1764. [CrossRef]
13. Tong, L.; Feng, Y.; Sun, X.; Han, Y.; Jiao, D.; Tan, X. High refractive index adamantane-based silicone resins for the encapsulation of light-emitting diodes. *Polym. Adv. Technol.* **2018**, *29*, 2245–2252. [CrossRef]
14. Macdonald, E.K.; Shaver, M.P. Intrinsic high refractive index polymers. *Polym. Int.* **2015**, *64*, 6–14. [CrossRef]
15. Lorentz, H.A. Ueber die Beziehung zwischen der Fortpflanzungsgeschwindigkeit des Lichtes und der Körperdichte. *Ann. Phys.* **1880**, *245*, 641–665. [CrossRef]
16. Lorenz, L. Ueber die refractionsconstante. *Ann. Phys.* **1880**, *247*, 70–103. [CrossRef]

17. Seferis, J.; Brandrup, J.; Immergut, E. *Polymer Handbook*; Wiley: New York, NY, USA, 1989; Volume 3, p. 45.
18. Hadis, M.A.; Tomlins, P.H.; Shortall, A.C.; Palin, W.M. Dynamic monitoring of refractive index change through photoactive resins. *Dent. Mater.* **2010**, *26*, 1106–1112. [CrossRef]
19. Su, M.; Sun, Y.; Chen, B.; Zhang, Z.; Yang, X.; Chen, S.; Pan, Q.; Zuev, D.; Belov, P.; Song, Y. A fluid-guided printing strategy for patterning high refractive index photonic microarrays. *Sci. Bull.* **2021**, *66*, 250–256. [CrossRef]
20. Tokushita, Y.; Watanabe, A.; Torii, A.; Nakabayashi, K.; Samitsu, S.; Mori, H. Photocurable selenophene/maleimide-based high-refractive-index copolymers obtained via radical copolymerization. *React. Funct. Polym.* **2021**, *165*, 104960. [CrossRef]
21. Okutsu, R.; Suzuki, Y.; Ando, S.; Ueda, M. Poly (thioether sulfone) with high refractive index and high Abbe's number. *Macromolecules* **2008**, *41*, 6165–6168. [CrossRef]
22. Pan, Z.; Zeng, K.; Huang, B.; Zhu, L. Synthesis of Hydrogen-Containing Methyl Phenyl Silicone Resins with a High Refractive Index for LED Encapsulation. *J. Electron. Mater.* **2020**, *49*, 4816–4821. [CrossRef]
23. Wadi, V.S.; Jena, K.K.; Halique, K.; Brigita, R.; Cmok, L.; Tzitzios, V.; Alhassan, S.M. Scalable High Refractive Index polystyrene-sulfur nanocomposites via in situ inverse vulcanization. *Sci. Rep.* **2020**, *10*, 14924. [CrossRef] [PubMed]
24. Jang, W.; Choi, K.; Choi, J.S.; Pyun, J.; Lim, J.; Char, K.; Im, S.G. One-step vapor-phase synthesis of transparent high refractive index sulfur-containing polymers. *Sci. Adv.* **2020**, *6*, eabb5320.
25. Catel, Y.; Angermann, J.; Fassler, P.; Fischer, U.; Schnur, T.; Moszner, N. High refractive index monofunctional monomers as promising diluents for dental composites. *Dent. Mater.* **2021**, *37*, 351–358. [CrossRef]
26. Zhao, X.; Li, S.; Liu, X.; Yang, X.; Zhang, Y.; Yu, R.; Zuo, X.; Huang, W. Synthesis and characterization of thianthrene-based epoxy with high refractive index over 1.7. *Phosphorus Sulfur Silicon Relat. Elem.* **2018**, *193*, 33–40. [CrossRef]
27. Zuo, J.; Liu, Z.; Luo, C.; Lin, F. Preparation and properties of high refractive index polythioetherimide film based on thiol-ene click chemistry. *Prog. Org. Coat.* **2021**, *151*, 106048. [CrossRef]
28. Hifumi, R.; Tomita, I. Synthesis and high refractive index properties of poly(thiophosphonate)s. *Polym. J.* **2018**, *50*, 467–471. [CrossRef]
29. Mavila, S.; Sinha, J.; Hu, Y.; Podgorski, M.; Shah, P.K.; Bowman, C.N. High Refractive Index Photopolymers by Thiol-Yne "Click" Polymerization. *ACS Appl. Mater. Interfaces* **2021**, *13*, 15647–15658. [CrossRef]
30. Jeong, M.K.; Choi, W.T.; Ahn, B.-H.; Gal, Y.-S.; Lim, K.T. High refractive index organic/inorganic hybrid films prepared by carbazole phenoxy based copolymers and titanium alkoxide. *Mol. Cryst. Liq. Cryst.* **2019**, *686*, 45–54. [CrossRef]
31. Lee, S.-H.; Kim, D.H.; Goh, M.; Kim, J.G.; You, N.-H. Synthesis and characterization of UV-Curable pyrimidine-based Poly(Acrylate) and zirconium acrylate nanocomposite with high refractive index. *Polymer* **2021**, *227*, 123847. [CrossRef]
32. Iino, S.; Sobu, S.; Nakabayashi, K.; Samitsu, S.; Mori, H. Highly transparent and photopatternable spirobifluorene-based polythioethers with high refractive indices via thiol-ene click chemistry. *Polymer* **2021**, *224*, 123725. [CrossRef]
33. Fu, M.C.; Ueda, M.; Ando, S.; Higashihara, T. Development of Novel Triazine-Based Poly(phenylene sulfide)s with High Refractive Index and Low Birefringence. *ACS Omega* **2020**, *5*, 5134–5141. [CrossRef] [PubMed]
34. Yao, B.; Hu, X.; Liu, J.; Chen, K.; Liu, J. Preparation and properties of high refractive index ZrO_2 nano-hybrid materials. *Mater. Lett.* **2020**, *261*, 126878. [CrossRef]
35. Lü, C.; Cui, Z.; Wang, Y.; Li, Z.; Guan, C.; Yang, B.; Shen, J. Preparation and characterization of ZnS–polymer nanocomposite films with high refractive index. *J. Mater. Chem.* **2003**, *13*, 2189–2195. [CrossRef]
36. Chen, X.; Fang, L.; Wang, J.; He, F.; Chen, X.; Wang, Y.; Zhou, J.; Tao, Y.; Sun, J.; Fang, Q. Intrinsic High Refractive Index Siloxane–Sulfide Polymer Networks Having High Thermostability and Transmittance via Thiol–Ene Cross-Linking Reaction. *Macromolecules* **2018**, *51*, 7567–7573. [CrossRef]
37. Legrand, S.; Hannu-Kuure, M.; Kärkkäinen, A. Design, preparation, and characterization of new high-refractive index hybrid organic–inorganic polysiloxanes: Innovative coatings for optoelectronic applications. *J. Appl. Polym. Sci.* **2020**, *138*, 49877. [CrossRef]
38. Dan, S.; Gu, H.; Tan, J.; Zhang, B.; Zhang, Q. Transparent epoxy/TiO_2 optical hybrid films with tunable refractive index prepared via a simple and efficient way. *Prog. Org. Coat.* **2018**, *120*, 252–259. [CrossRef]
39. Yang, H.; Zhou, M.; Tang, H.; Sun, M.; Liu, P.; Liu, Y.; Chen, L.; Li, D.; Wu, D.; Hao, J.; et al. Enhanced light emission of quantum dot films by scattering of poly(zinc methacrylate) coating CdZnSeS/ZnS quantum dots and high refractive index $BaTiO_3$ nanoparticles. *RSC Adv.* **2020**, *10*, 31705–31710. [CrossRef]
40. Wildner, W.; Drummer, D. Nanofiller materials for transparent polymer composites: Influences on the properties and on the transparency—A review. *J. Thermoplast. Compos. Mater.* **2019**, *32*, 1547–1565. [CrossRef]
41. Shen, L.; Li, Y.; Zheng, J.; Lu, M.; Wu, K. Modified epoxy acrylate resin for photocurable temporary protective coatings. *Prog. Org. Coat.* **2015**, *89*, 17–25. [CrossRef]
42. Cheng, F.; Fan, Y.; Zhang, L.; Jiao, X.; Lai, G.; Hua, X.; Yang, X. An Easy Fabrication Method to Prepare Inexpensive UV–Cured Transparent Silicone Modified Polyacrylate Coatings with Good Adhesion and UV Resistance. *Coatings* **2020**, *10*, 675. [CrossRef]
43. Vang, K.C.; Yu, T.H.; David, M. *52.5: Broadband Antireflection (BBAR) Nanostructure Contrast Enhancement (NCEF) Films For Electronic Optical Display Applications*; SID Symposium Digest of Technical Papers; Blackwell Publishing Ltd.: Oxford, UK, 2011; pp. 770–772.
44. Ostrovsky, N.; Yehuda, D.; Tzadka, S.; Kassis, E.; Joseph, S.; Schvartzman, M. Direct Imprint of Optical Functionalities on Free-Form Chalcogenide Glasses. *Adv. Opt. Mater.* **2019**, *7*, 1900652. [CrossRef]
45. Li, S.; Li, X.; Zhong, M.; Lu, Y.; Jiajie, Y.; Yongmin, Z.; He, X. Synthesis of NSAIDs–Se derivatives as potent anticancer agents. *Med. Chem. Res.* **2018**, *27*, 2071–2078. [CrossRef]

46. Zhao, J.; Liu, C.; Li, Y.; Liang, J.; Liu, J.; Qian, T.; Ding, J.; Cao, Y.C. Preparation of carbon quantum dots based high photostability luminescent membranes. *Luminescence* **2017**, *32*, 625–630. [CrossRef]
47. Tang, S.; Lan, Q.; Xu, L.; Liang, J.; Lou, P.; Liu, C.; Mai, L.; Cao, Y.-C.; Cheng, S. A novel cross-linked nanocomposite solid-state electrolyte with super flexibility and performance for lithium metal battery. *Nano Energy* **2020**, *71*, 104600. [CrossRef]
48. Guo, S.; Lv, Y.; Chen, Y.; Cai, S. Amine-containing olefin copolymer with CO_2-switchable oil absorption and desorption. *J. Appl. Polym. Sci.* **2019**, *136*, 47439. [CrossRef]
49. Wei, Y.; Su, Y.; Liu, C.; Nie, X.; Liu, Z.; Zhang, Y.; Zhang, Y. Two-channel SPR sensor combined application of polymer-and vitreous-clad optic fibers. *Sensors* **2017**, *17*, 2862. [CrossRef]
50. Xia, Y.; Liang, X.; Jiang, Y.; Wang, S.; Qi, Y.; Liu, Y.; Yu, L.; Yang, H.; Zhao, X.Z. High-Efficiency and Reliable Smart Photovoltaic Windows Enabled by Multiresponsive Liquid Crystal Composite Films and Semi-Transparent Perovskite Solar Cells. *Adv. Energy Mater.* **2019**, *9*, 1900720. [CrossRef]
51. Lv, R.; Bei, Z.; Huang, Y.; Chen, Y.; Zheng, Z.; You, Q.; Zhu, C.; Cao, Y. Mussel-Inspired Flexible, Wearable, and Self-Adhesive Conductive Hydrogels for Strain Sensors. *Macromol. Rapid Commun.* **2020**, *41*, 1900450. [CrossRef]
52. Pan, G.; Du, Z.; Zhang, C.; Li, C.; Yang, X.; Li, H. Synthesis, characterization, and properties of novel novolac epoxy resin containing naphthalene moiety. *Polymer* **2007**, *48*, 3686–3693. [CrossRef]
53. Yan, R.; Yang, D.; Zhang, N.; Zhao, Q.; Liu, B.; Xiang, W.; Sun, Z.; Xu, R.; Zhang, M.; Hu, W. Performance of UV curable lignin based epoxy acrylate coatings. *Prog. Org. Coat.* **2018**, *116*, 83–89. [CrossRef]
54. Chen, K.; Tian, C.; Cao, F.; Liang, S.; Jia, X.; Wang, J. Preparation and characterization of highly thermostable polyisocyanurate foams modified with epoxy resin. *J. Appl. Polym. Sci.* **2016**, *133*, 43085. [CrossRef]
55. Pal, R.; Sudhi, S.; Raghavan, R. Fabrication and evaluation of structural film adhesive using oxazolidinone modified novolac epoxy resin. *J. Appl. Polym. Sci.* **2019**, *136*, 47520. [CrossRef]
56. Chian, K.; Yi, S. Synthesis and characterization of an isocyanurate–oxazolidone polymer: Effect of stoichiometry. *J. Appl. Polym. Sci.* **2001**, *82*, 879–888. [CrossRef]
57. Pretorius, F.; Focke, W.W.; Androsch, R.; du Toit, E. Estimating binary liquid composition from density and refractive index measurements: A comprehensive review of mixing rules. *J. Mol. Liq.* **2021**, *332*, 115893. [CrossRef]
58. Carnegie, M.R.; Sherine, A.; Sivagami, D.; Sakthivel, S. Anti-reflection coatings with enhanced abrasion and scratch resistance properties. *J. Sol-Gel Sci. Technol.* **2016**, *78*, 176–186. [CrossRef]
59. Sprokel, G.; Santo, R.; Swalen, J. Determination of the surface tilt angle by attenuated total reflection. *Mol. Cryst. Liq. Cryst.* **1981**, *68*, 29–38. [CrossRef]